Build Simul
DOI 10.1007/s12273-008-8115-y

RESEARCH ARTICLE

Study of Cooling System with Water Mist Sprayers: Fundamental Examination of Particle Size Distribution and Cooling Effects

Hideki Yamada[1], Gyuyoug Yoon[1](✉), Masaya Okumiya[1], Hiroyasu Okuyama[2]

1. Graduate School of Environmental Studies, Nagoya University, Furo-cho, Chikusa-ku, Nagoya-shi, Aichi 464-8603, Japan
2. Institute of Technology, Shimizu Corporation, 3-4-17, Etchujima, Koto-ku, Tokyo 135-8530, Japan

Received: 23 November 2007 / Revised: 25 April 2008 / Accepted: 16 May 2008

Abstract A cooling system that sprays micro water droplets could prove useful in mitigating temperature increases in urban areas by using the heat of water evaporation, a process that consumes only small amounts of water and energy. If water mist is sprayed in a semi-outdoor area, for example, under a canopy, it could potentially improve conditions on hot days. However, there is little reference data concerning the design or control of such systems. In order to propose a method for designing and predicting the performance of a water mist system, we discuss differences in cooling effects in the context of particle size distribution of water mist. The results of numerical fluid analysis showed there is no significant difference in temperature reduction for different particle sizes. However, the water particles remained in a lower position with larger particles.

Keywords water mist, evaporative cooling, urban heat island, numerical fluid analysis

List of symbols

a_{gs}	solar absorptance at ground surface (—)
A	surface area (m^2)
c	heat capacity (J/(kg·K))
d	droplet diameter (m)
d_L	ligament diameter (m)
d_{inj}	injector orifice diameter (m)
d_0	most probable droplet size (m)
d_{ug}	depth (m)
$\bar{d}$	size constant (m)
f_D	drag force coefficient (s^{-1})
f_x	additional force coefficient (m/s^2)
F	momentum (N·m/s)
h	film thickness (m)
J	horizontal solar radiation (W/m^2)
k_m	mass transfer coefficient (m/s)
K_b	the most unstable wavelength (s^{-1})
l	latent heat (J/kg)
L_b	breakup length (m)
m	mass (kg)
$\dot{m}$	mass flow rate (kg/s)
M	molecular weight (kg/mol)
n	spread parameter of a Rosin-Rammler distribution (—)
N	molar flux of vapor (mol/(m^2·s))
Oh	Ohnesorge number
p	vapor pressure (Pa)
q_{cond}	heat diffusion to the underground (W/m^2)
q_{conv}	heat convection and long-wavelength radiation (W/m^2)
q_{sol}	transmissive solar radiation (W/m^2)
R	universal gas constant (Pa·m^3/(mol·K))
t	time (s)
T	temperature (K)
u	velocity (m/s)
v	axial component of sheet velocity (m/s)
V	total sheet velocity (m/s)
X_i	local bulk mole fraction of species i (—)
Y_d	mass fraction of droplets with diameter greater than d (—)
α	heat transfer coefficient (W/(m^2·K))

E-mail: yoonq4@hotmail.com

η	wave amplitude (m)
θ	spray angle measured from spray axis (rad)
λ	thermal conductivity (W/(m·K))
ρ	density (kg/m^3)
τ	solar transmittance (—)
Ω	growth of the most unstable wave (s^{-1})

Subscripts

0	at the injector exit
air	air property
b	sheet breaks up
g	gas property
gs	ground surface
l	liquid property
L	liquid ligament
i	vapor species
p	particle
rf	roof surface
sat	saturated condition
ug	under ground

1 Introduction

In recent years, warming of urban areas in summer has become a problem known as the "urban heat island effect". One means of mitigating this effect is to spray micro water droplets. This method suppresses the temperature rise in urban areas by using the heat of water evaporation, while using only small amounts of water and energy. If water mist is sprayed in a semi-outdoor area, for example, under a canopy, it could potentially improve conditions on hot days. Through a field experiment (Yamada et al. 2006), we have verified the effectiveness of this method and confirmed a temperature reduction under a canopy of up to about 3℃. Such water mist systems are expected to be used increasingly in the future, yet there is little reference data concerning the design or control of such systems. Therefore, this study proposes a method for designing and predicting the performance of water mist systems. In this study, we conducted a numerical fluid analysis and then examined the particle size distribution and the cooling effect of water mist.

2 Simulation Outline

In this study, the simulations were conducted by using a CFD (computational fluid dynamics) code Fluent. And, we used discrete phase model (DPM) for calculating momentum, heat and mass exchange between the water mist and the air. Also, we adapted the pressure-swirl atomizer model in this simulation. DPM and the pressure-swirl atomizer model have been mounted in Fluent basically. In Section 2.1 and 2.2, we described these models by quoting the user's manual (Fluent 2006). And, we presented calculation conditions of simulations in Section 2.3.

2.1 Discrete phase model

We adopted the discrete phase model (DPM) that it allows to simulate a discrete second phase in a Lagrangian frame of reference in addition to solving transport equations for the continuous phase. Also, DPM can compute the trajectories of the discrete phase entities, as well as momentum transfer, heat and mass transfer to/from them (Fig. 1).

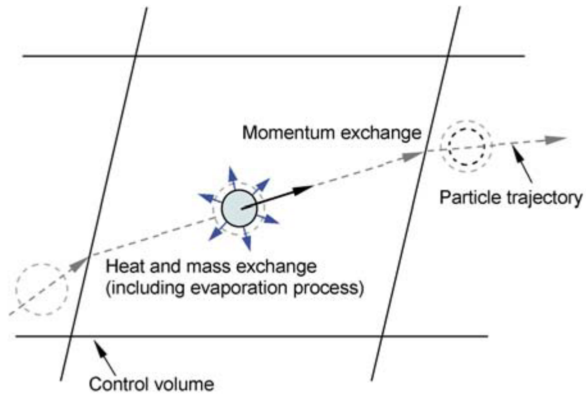

Fig. 1 Diagram of discrete phase model

Momentum exchange

The momentum transfer from the continuous phase to the discrete phase is computed by examining the change in momentum of a particle as it passes through each control volume. The trajectory of a discrete phase particle is predicted by integrating the force balance on the particle, which is written in a Lagrangian reference frame. This momentum balance is given by

$$F_\mathrm{p}=\frac{\mathrm{d}u_\mathrm{p}}{\mathrm{d}t}m_\mathrm{p}\Delta t=\left(f_\mathrm{D}(u_\mathrm{g}-u_\mathrm{p})+\frac{g(\rho_\mathrm{p}-\rho_\mathrm{g})}{\rho_\mathrm{p}}+f_x\right)m_p\Delta t, \quad (1)$$

here, f_x is the additional acceleration (force/unit particle mass), $f_\mathrm{D}(u_\mathrm{g}-u_\mathrm{p})$ is the drag force per unit particle mass term.

Heat and mass exchange

The heat exchange according to convective and latent heat transfer is given by

$$m_\mathrm{p}c_\mathrm{p}\frac{\mathrm{d}T_\mathrm{p}}{\mathrm{d}t}=\alpha A_\mathrm{p}(T_\mathrm{g}-T_\mathrm{p})+\frac{\mathrm{d}m_\mathrm{p}}{\mathrm{d}t}l. \quad (2)$$

The mass of droplet is reduced according to

$$\frac{\mathrm{d}m_\mathrm{p}}{\mathrm{d}t}=-N_iA_\mathrm{p}M_i, \quad (3)$$

where N_i is the molar flux of vaporize species, H_2O in this study, given by

$$N_i = k_{\mathrm{m}}\left(\frac{p_{\mathrm{sat}}(T_{\mathrm{p}})}{RT_{\mathrm{p}}} - X_i \frac{p_{\mathrm{g}}}{RT_{\mathrm{g}}}\right). \tag{4}$$

The evaporation of water mist is computed by this mass exchange and latent heat transfer.

2.2 Atomizer model and droplet size distribution

Atomizer model

In this study, the pressure-swirl atomizer is used. This atomizer accelerates the liquid through nozzles known as swirl ports into a central swirl chamber. As shown in Fig. 2, the swirling liquid pushes against the walls of the swirl chamber and develops a hollow air core. It then emerges from the orifice as a thinning sheet, which is unstable, breaking up into ligaments and droplets (Schmidt et al. 1999). The most probable droplet size spout atomizer is calculated by a series of following equations.

Film formation

The centrifugal motion of the liquid within the injector creates an air core surrounded by a liquid film. The thickness of this film, h_0, is given by

$$h_0 = \frac{1}{2}\left(d_{\mathrm{inj}} - \sqrt{d_{\mathrm{inj}} - \frac{4\dot{m}_l}{\pi\rho_l v}}\right), \tag{5}$$

where d_{inj} is the injector orifice diameter, and $\dot{m}_l$ is the effective mass flow rate, v is the axial component of velocity at the injector exit. The axial component of velocity at the injector exit is calculated by

$$v = V\cos\theta, \tag{6}$$

where V is total velocity of axial and tangential velocity, θ is the spray angle.

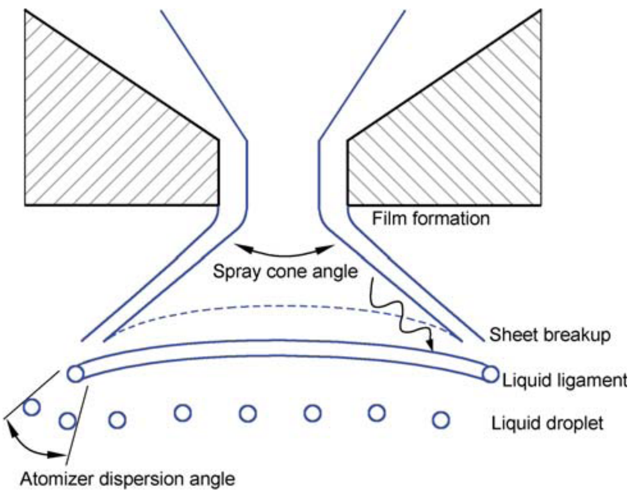

Fig. 2 Formation of liquid droplet for pressure-swirl atomizer model

The total velocity V is determined by the fluid pressure and the injector orifice diameter.

Sheet breakup

The wavy disturbances occur on the liquid film; the sheet breaks up and ligaments will be formed at a length given by

$$L_{\mathrm{b}} = \frac{V}{\Omega}\ln\left(\frac{\eta_{\mathrm{b}}}{\eta_0}\right), \tag{7}$$

where the quantity $\ln(\eta_{\mathrm{b}}/\eta_0)$ is an empirical sheet constant. The default value of 12 was obtained theoretically (Dombrowski and Hooper 1962). Ω is the maximum growth rate of wave that occurred into the liquid film.

Atomization

If it is assumed that the ligaments are formed from tears in the sheet twice per wavelength, the resulting diameter is given by

$$d_{\mathrm{L}} = \sqrt{\frac{8h_{\mathrm{b}}}{K_{\mathrm{b}}}}, \tag{8}$$

$$h_{\mathrm{b}} = \frac{(d_{\mathrm{inj}} - h_0)h_0}{\left(d_{\mathrm{inj}} - h_0 + 2L_{\mathrm{b}}\sin\left(\frac{\theta}{2}\right)\right)}. \tag{9}$$

The most probable droplet size d_0 is calculated by

$$d_0 = 1.88 d_{\mathrm{L}}(1 + 3Oh)^{1/6}, \tag{10}$$

here, Oh is the Ohnesorge number which is a combination of the Reynolds number and the Weber number. It can be supposed d_0 corresponds to volumetric mean diameter of generated entire droplets.

Droplet size distribution

The particle size distribution is determined by Rosin-Rammler diameter distribution method when the pressure-swirl atomizer model is used. According to Institute for Liquid Atomization and Spray System—Japan (2001), the mass fraction of droplets of diameter greater than d is given by

$$Y_d = \exp(-(d/\bar{d})^n), \tag{11}$$

where d is the droplet diameter, $\bar{d}$ is the size constant, n is the distribution parameter. When the pressure-swirl atomizer model is used, n should be given by default value of 3.5. This expression can be inverted by taking logs of both sides and rearranging

$$\bar{d} = \frac{d}{(-\ln(Y_d))^{\frac{1}{n}}} \tag{12}$$

here, substituting d_0 for d, Y_d is to be 0.92. Because d_0

corresponds to volumetric mean diameter, this equation is to be

$$\bar{d} = 2.03 d_0 \tag{13}$$

Then, Eq. (11) can be rewritten as

$$Y_d = \exp(-(d/2.03 d_0)^n) \tag{14}$$

So, if the value of d_0 was determined, we can obtain the droplet size distribution as shown in Fig. 3.

2.3 Calculation area and boundary conditions

The semi-outdoor area is 50m long, 15m wide and 4m high as shown in Fig. 4, and was analyzed assuming that it is being used as a waiting area at an event hall. The boundary conditions in Table 1 were given. Air temperature and humidity in the area were given with typical summer day in Tokyo (air temperature of 33.4℃, humidity of 58%RH). It was also assumed that there was airflow (wind velocity of 0.1m/s) of outdoor wind. The roof was made of PVC-coated glass-fiber and the ground was covered by concrete; those material properties are shown in Table 2. Sol-air temperature and thermal transmittance were given for the roof surface. At the ground surface, the ground surface temperature was given. The ground surface temperature was estimated in consideration of heat transfer at the ground surface as shown in Fig. 5.

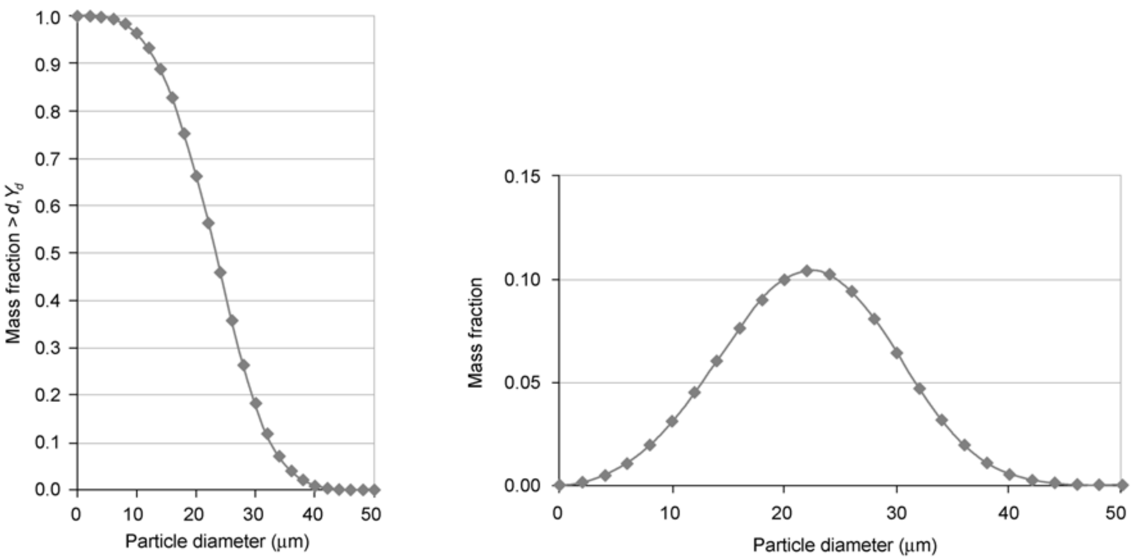

Fig. 3 Example of particle diameter distribution: (a) cumulative size distribution of particles, (b) particle size distribution

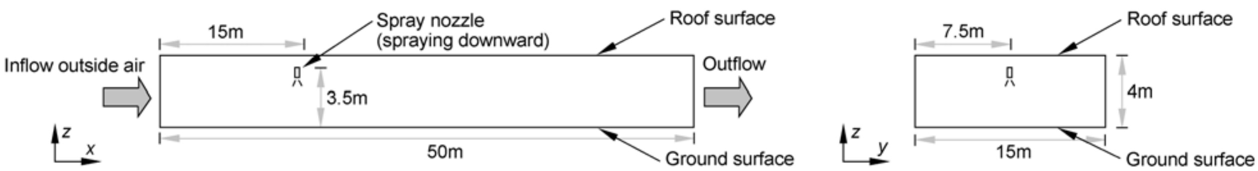

Fig. 4 Diagram of calculation area

Table 1 Boundary conditions

Boundary	Momentum condition	Thermal condition
Roof surface (z = 4m)	No-slip	External air temperature[a]: 38.2℃ External heat transfer coefficient: 23W/(m^2·K)
Ground surface (z = 0)	No-slip	Surface temperature: 29.8℃
Inflow outside air (x = 0)	Inflow velocity: 0.1m/s	Outside temperature: 33.4℃ Outside humidity: 18.9g/kg(DA)
Outflow (x = 50m)	Pressure: atmospheric pressure	Outside temperature: 33.4℃ Outside humidity: 18.9g/kg(DA)
Side surface (y = 0, y = 50m)	Free-slip	Adiabatic boundary

[a]Sol-air temperature was given. It assumed that the horizontal solar radiation is 1.026kW/m^2.

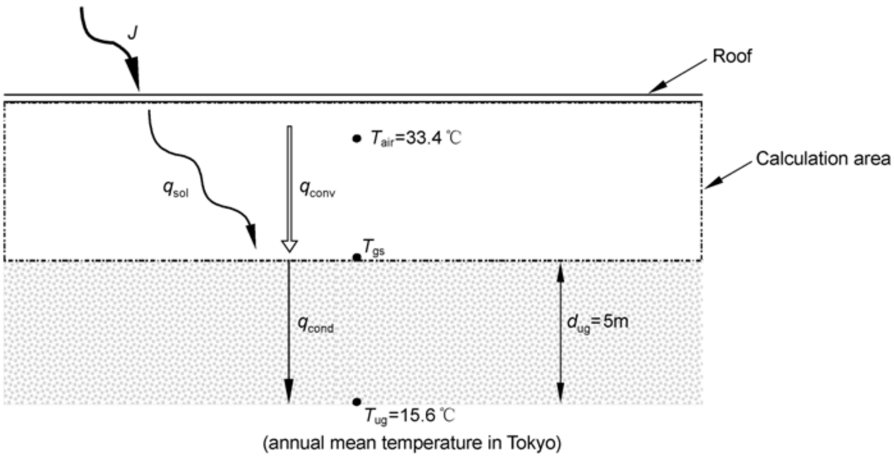

Fig. 5 Heat balance at the ground surface

The heat balance at the ground surface is

$$q_{\mathrm{conv}} + q_{\mathrm{cond}} + q_{\mathrm{sol}} = 0, \tag{15}$$

$$q_{\mathrm{conv}} = \alpha(T_{\mathrm{air}} - T_{\mathrm{gs}}), \tag{16}$$

$$q_{\mathrm{cond}} = \frac{\lambda_{\mathrm{ug}}}{d_{\mathrm{ug}}}(T_{\mathrm{ug}} - T_{\mathrm{gs}}), \tag{17}$$

$$q_{\mathrm{sol}} = \tau_{\mathrm{rf}} a_{\mathrm{gs}} J, \tag{18}$$

here, q_{conv} is the heat convection and long-wavelength radiation from the air to the ground surface, q_{cond} is the heat diffusion to the underground, q_{sol} is the solar radiation after penetrating the roof to the ground.

Table 3 lists the spraying conditions of the atomizer. For this study, only the sheet constant was varied in order to generate different particle size distributions under the same spray conditions. Figure 6 and Table 4 show the particle size distributions for the three cases considered in this analysis.

The CFD simulation in this study is based on conservation equations of energy, mass, and momentum of incompressible air. Also, this simulation adopted the standard k-ε turbulence model. The grid distance in each axial set to be 0.5 – 1.0m and the entire calculation domain is composed a total of 11,200 cells. We conducted unsteady simulation until the fluctuation of average air temperature in the calculation domain is smaller than 10^{-6} K.

Table 2 Material properties for the roof and ground surface

Roof surface (z = 4m)	Material: PVC-coated glass-fiber plain-weave
	Thickness: 0.53mm
	Thermal conductivity: 0.11W/(m·K)
	Solar absorptance: 10.8%
	Solar transmittance: τ_{rf} = 13.7%
Ground surface (z = 0)	Material: paved concrete
	Thickness: d_{ug} = 5m
	Thermal conductivity: λ_{ug} = 1.4W/(m·K)
	Solar absorptance: a_{gs} = 60.0%

Table 3 Spraying conditions

Mass flow rate	0.83g/s
Water temperature	33.4℃
Injector orifice diameter	0.16mm
Spray cone angle	50°
Atomizer dispersion angle	6°
Injection pressure	6MPa

Table 4 Sheet constant and the representative droplet diameter

	Case 1	Case 2	Case 3
Sheet constant	24	12	6
Volumetric mean diameter (μm)	9.0	12.7	17.9
Sauter mean diameter (μm)	16.9	20.8	32.6

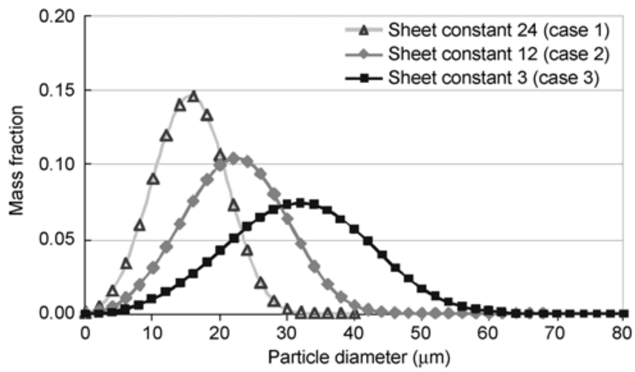

Fig. 6 Particle size distributions

3 Analysis result and discussion

3.1 Single-nozzle: results and discussion

Figures 7 to 9 show the vertical cross-section temperature contours at the spray location (y = 7.5m) for the three cases. Figures 10 and 11 show the temperature distribution and the absolute humidity distribution at 1.5m ($y = 7.5$m, $z = 1.5$m) above the ground. For each case, the air temperature decreased about 1.5℃ at the spray location ($x \approx 15$m). Also, about 2.5m behind the spray position, it was observed that the maximum air temperature increase was about 0.5℃. It was thought that this phenomenon is caused by the downward airflow from the mist spray position. The wind direction diagram shown in Fig. 12 also confirms this phenomenon. Also, there was no significant temperature reduction at the position behind the spray location ($x = 20-50$m). The absolute humidity increased to about 20.0g/kg (DA) at the spray location to only about 19.2 to 19.5g/kg (DA) at the position behind the spray location, representing an increase of 0.3 to 0.6g/kg (DA). Figure 13 shows the remaining particle mass distribution at every height of the analysis area. The total mass of remaining particles was smaller for case 1 than for the other two cases, indicating a fast evaporation rate. In case 3, which was for comparatively large particles, there was a large mass of particles remaining in the area. When the mass of remaining particles was analyzed as a function of height, the particles remained even at a height of 1.4m.

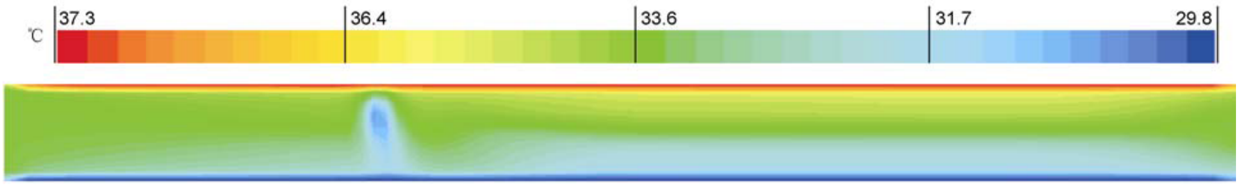

Fig. 7 Case 1, air temperature contours at the spray location ($y = 7.5$m)

Fig. 8 Case 2, air temperature contours at the spray location ($y = 7.5$m)

Fig. 9 Case 3, air temperature contours at the spray location ($y = 7.5$m)

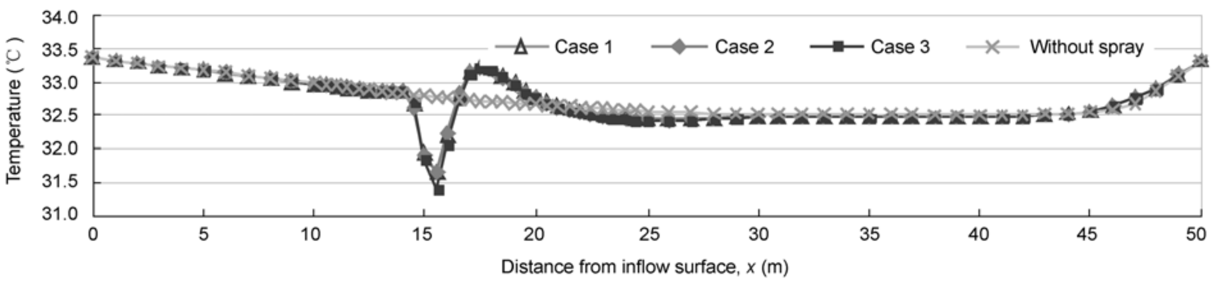

Fig. 10 Air temperature distribution at the spray location of 1.5m height

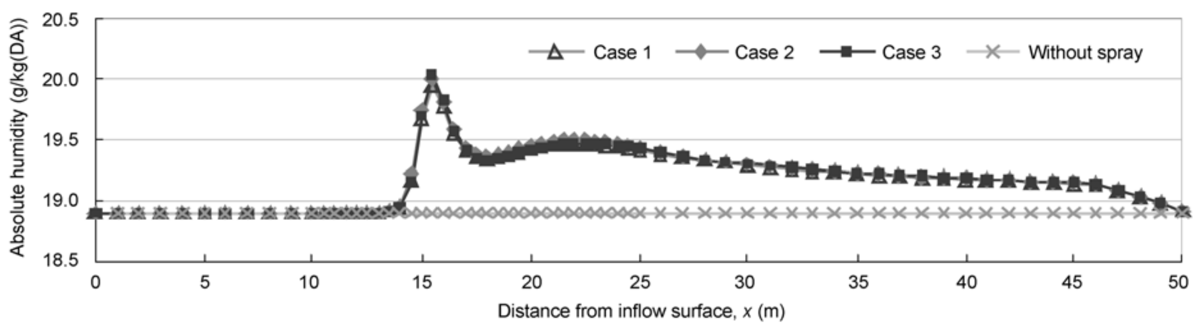

Fig. 11 Absolute humidity distribution at the spray location of 1.5m height

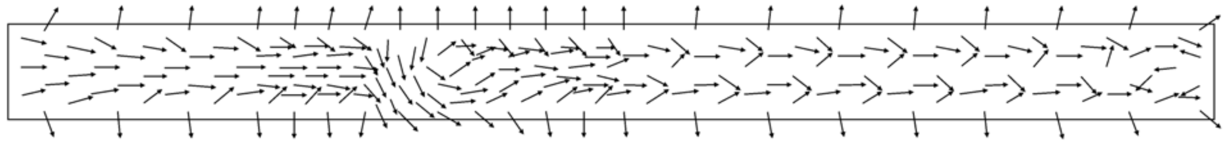

Fig. 12 Airflow direction at spray location ($y = 7.5$m)

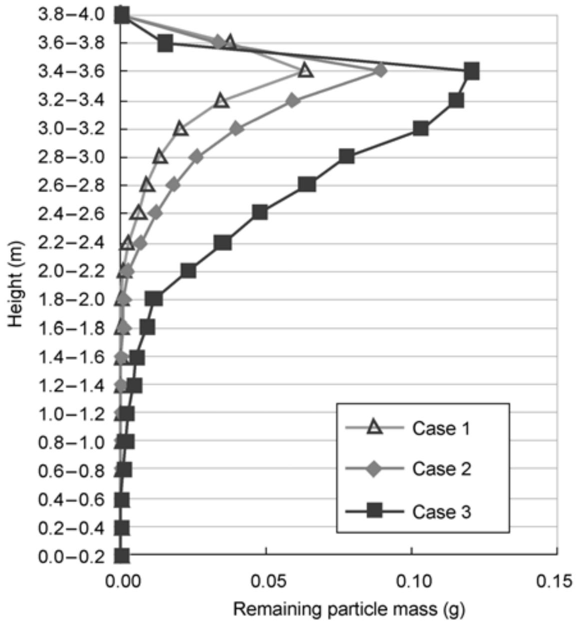

Fig. 13 Remaining particle mass distribution at each height

These results revealed that the temperature reduction does not vary greatly with differences in particle size distribution. However, as the particle size increases, it takes longer time for the particles to completely evaporate, and particles may remain even at low heights. Thus, the particle size is an important parameter in mist design when considering the spray height.

3.2 Multiple nozzles: results and discussion

This section discusses the effect of particle size distribution when multiple nozzles were arranged at same intervals. The same calculation conditions were used as for the single-nozzle scenario. Three nozzles were used, and the 2nd and 3rd were installed at 2.5m intervals from the single-nozzle spray position in order to reduce the temperature increase behind the spray position. Only cases 2 and 3, which had large particles, were simulated. Also, cases 2' and 3' had the same particle size distributions as cases 2 and 3, respectively. Figures 14 and 15 show the cross-sectional ($y = 7.5$m) temperature contours for cases 2' and 3'. Figures 16 and 17 show the air temperature distribution and the absolute humidity distribution at a height of 1.5m ($y = 7.5$m, $z = 1.5$m). Similarly to the case of the single nozzle, there was no significant difference in the temperature reduction for different particle size distributions. The air temperature just below each nozzle was about 31.3℃, which was approximately equal to that in the case of a single nozzle. Compared with the absolute humidity distribution, the humidity just below the 1st nozzle was similar to the single-nozzle case. However, the humidity just below the nozzle further behind was higher than that below the nozzle further ahead. The humidity of the 3rd nozzle was about 0.2g/kg (DA) greater than that for the corresponding case of the single nozzle.

Figures 18 and 19 show the horizontal distribution of air temperature at a height of 1.5m for cases 2 and 2'. In the cases where multiple nozzles were used, the air temperature in front of the 1st nozzle was lower than with the single nozzle. The cause of the difference of temperature distribution was considered to be that the downward flow by water mist evaporation was greater than in the case of the single nozzle, and that the heat of mist vaporization was diffused more easily because of the downflow due to mist blocking the inflow of outdoor air. This phenomenon may have occurred because the side boundary condition was a wall without new air inflow or outflow.

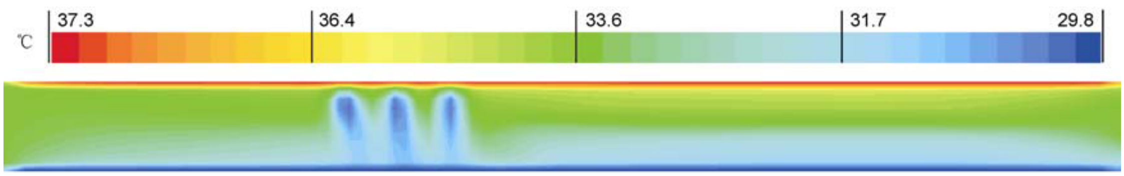

Fig. 14 Case 2', air temperature contours at the spray location ($y = 7.5$m)

Fig. 15 Case 3', air temperature contours at the spray location ($y = 7.5$m)

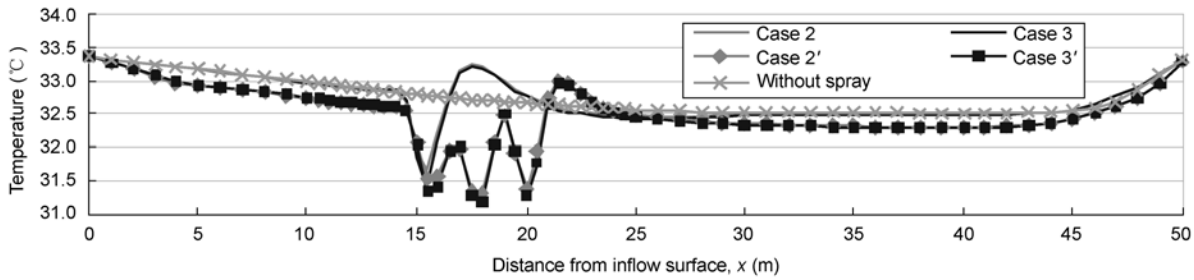

Fig. 16 Air temperature distribution at the spray location of 1.5m height

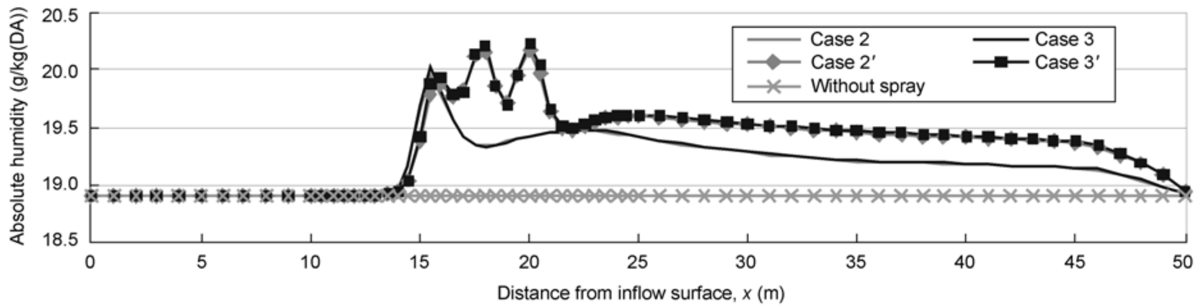

Fig. 17 Absolute humidity distribution at the spray location of 1.5m height

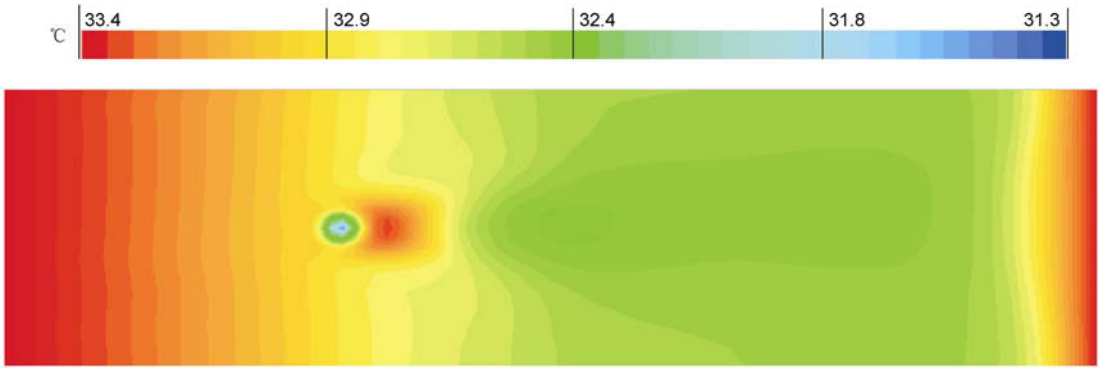

Fig. 18 Horizontal distribution of air temperature at a height of 1.5m with a single nozzle (case 2)

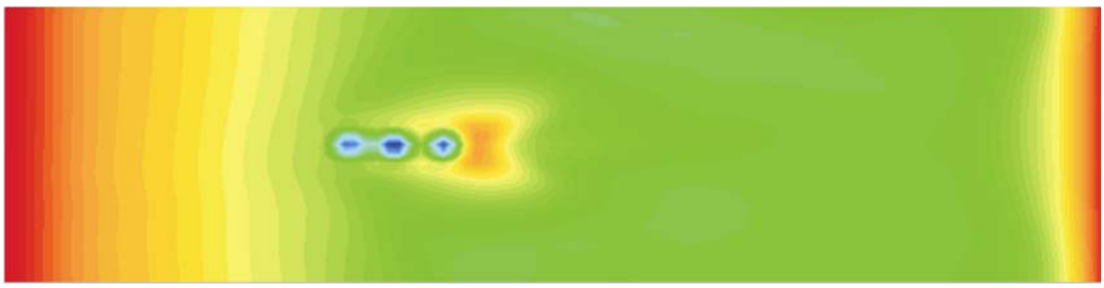

Fig. 19 Horizontal distribution of air temperature at a height of 1.5m with three nozzles (case 2')

Figure 20 shows the particle mass distribution at different heights. In comparing the cases of single and multiple nozzles, we see that the maximum mass of remaining particles was found to be at almost the same height. As for the minimum height at which particles remained, however, few particles remained at a height of 1.8m or lower in both cases 2 and 2', which had comparatively small particles. Comparing cases 3 and 3', which had comparatively large particles, a few particles remained even at a height of 1.0m for case 3'.

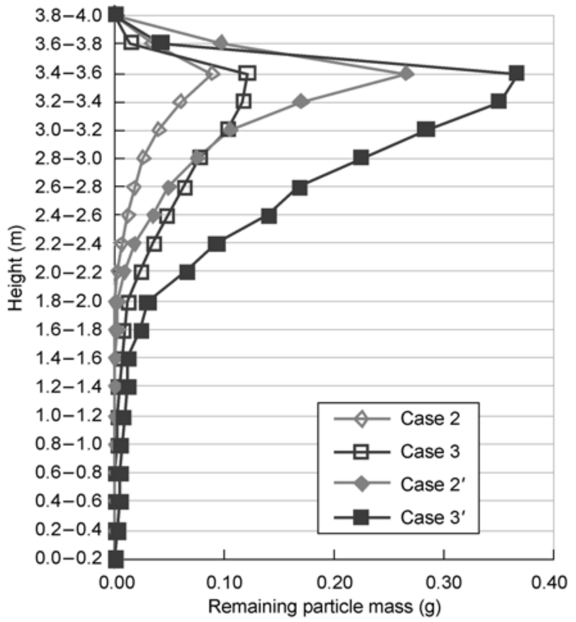

Fig. 20 Remaining particle mass distribution at each height

4 Conclusions

In this study, we discussed the cooling effect in terms of particle size distribution and the height distribution of remaining particles. A significant difference in temperature reduction for different particle size distributions was not observed. As the particle size increased, however, the minimum height of remaining particles was lower. In the case of single nozzle, there is no significant difference in the minimum height of remaining particles between case 1 (Sauter mean diameter 16.9μm) and case 2 (20.8μm). However, mist particles remained at lower heights in case 3 (Sauter mean diameter of 32.6μm). Thus, when the different particle size was larger than a dozen micrometer, it is expected to make a relatively larger effect on the height of remaining particles. Also, mist particles remained at lower heights when the number of nozzles was increased. The above results demonstrate that spray height and particle size need to be selected carefully while the height of remaining particles is to be strictly controlled.

For those cases (spray particle size is Sauter mean diameter 16.9μm, 20.8μm and 32.6μm), the air temperature reduction was same with that of these field experiments (Hayashi et al. 2005; Yamada et al. 2006). That is to say, the simulation in this study could reproduce the evaporation cooling effect of mist spray system. In the future, we will confirm the validity of this simulation technique by considering the temperature reduction and the minimum height of remaining particles.

References

Dombrowski N, Hooper PC (1962). The effect of ambient density or drop formation in sprays. *Chemical Engineering Science*, 17: 291 – 305.

Fluent Inc. (2006). Fluent 6.3 User's Guide. http://www.ansys.com.

Hayashi A, Kodama N, Okuyama H, Tsujimoto M, Okumiya M, Harada M, Ichinose S, Shindo Y (2005). Development of heat island control system with water mist sprayer Part 3: Field measurement and computational fluid dynamics calculation. Summaries of technical papers of the annual meeting of the Architectural Institute of Japan, Kinki. (in Japanese)

Institute for Liquid Atomization and Spray Systems—Japan (2001). Atomization Technology. Morikita Publishing Co. (in Japanese)

Schmidt DP, Nouar I, Senecal PK, Hoffman J, Rutland CJ, Martin J, Reitz RD (1999). Pressure-swirl atomization in the near field. SAE technical paper, 1999-01-0496.

Yamada H, Okumiya M, Tsujimoto M, Harada M (2006). Study on the cooling effects of water mist sprayer. Summaries of technical papers of the annual meeting of the Architectural Institute of Japan, Kanto. (in Japanese)